Development of nascent focal adhesions in spreading cells

Abstract

The eukaryotic cell develops organelles in order to sense and respond to the mechanical properties of its surroundings. These mechanosensing organelles aggregate into symmetry-breaking patterns to mediate cell motion and differentiation on substrate. The spreading of a cell plated onto a substrate is one of the simplest paradigms in which angular symmetry-breaking assemblies of mechanical sensors are seen to develop. We review evidence for the importance of the edge of the cell-extracelullar matrix adhesion area in the aggregation of mechanosensors, and develop a theoretical model of mechanosensors clustering into nascent focal adhesions on this contact ring. To study the spatial patterns arising on this topological feature, we use a 1D lattice model with the nearest-neighbor interaction between individual integrin-mediated mechanosensors. We find the effective Ginzburg-Landau free energy for this model, and determine the spectrum of spatial modes as the cell spreads and increases its contact area with the substrate. To test our model, we compare its predictions with measured distributions of paxillin in spreading fibroblasts.

STATEMENT OF SIGNIFICANCE. Numerous theoretical, experimental and computer simulation studies have recently probed the mechanisms and signalling pathways mediating the response of a eukaryotic cell to interactions with a substrate. Integrin-based adhesion complexes are known to be the individual units controlling mechanical sensing, and their dense aggregation into focal adhesions leads to cells developing polarity, and eventually - locomotion. Here we develop a theoretical model that suggests that physical interactions between individual adhesion complexes, mediated by a double-functional protein, is the factor that defines the initial breaking of symmetry of the cell spreading on a substrate, and predicts the characteristic period of modulation above the critical size of the adhesion area.

1 Introduction

Most eukaryotic cells respond to external physical stimuli, and exert forces on surrounding cells and the extracellular matrix (ECM). They do this by substantially changing their overall shape, and developing localized mechanosentive and mechanotransducive organelles, such as focal adhesions (FAs), stress fibres and motile membrane protrusions (1, 2). These morphological changes can be rapid and may help to determine the behavior of the cell, including how it differentiates (3), moves (4, 5) and proliferates (6).

A cell becomes less symmetric when subjected to external physical and chemical cues (7). Indeed, eukaryotic cells become polarised during chemotaxis (8) and durotaxis (9, 10). Molecular pathways for both of these mechanisms are currently under investigation (11, 12), and a full network of interactions between the known components of the integrin adhesome underpinning durotaxis has been identified (13). However, we lack a detailed understanding of how (or rather - why) their individual sensors arrange themselves spatially. To progress with this problem, one needs a physical model accounting for the assembly of the force sensing and force transduction machinery within a generic cell.

Attempting such an analysis in a general geometry with a complex set of external cues is very complicated. Here we begin by reducing the problem down to the simplest possible (while still experimentally viable) configuration, which displays a defined allosteric organization of the constituent molecules. This paper is organized as follows: in the next section, which continues the Introduction, we summarize the biological background of the problem, and identify the key elements that will define our mathematical model. Section 3 (Methods) explains how we construct the model: we start with the interaction Hamiltonian, sum the partition function to obtain the effective free energy of the problem, and express it as a function of the inhomogeneous local density of individual mechanosensors. This section also examines the key approximations and limitations of the model, while the details of analysis are given in Supplementary Information. Section 4 presents the results of the model, which predicts the critical size of the expanding cell when the instability occurs and the characteristic period

0006-3495/08/09/2624/12 $2.00 doi: 10.1529/biophysj.106.090944

of emerging dense clusters of mechanosensors. This section also compares model predictions with experimental data: specifically, we find that a typical fibroblast on a flat substrate would generate about 100 nascent FAs, before they further coarsen into a few well-developed FAs. We conclude with a more general discussion of the limitations of our model and of its broader biological relevance.

2 Biological background

The same mechanosensitive organelles assemble regardless of whether or not the cell is subjected to large scale physical gradients (*e.g.* of stiffness and force). Moreover, cells placed in a homogeneous medium can still undergo stiffness-induced differentiation and, more remarkably, they can change their shape to allow for short periods of straight-line motion (14). The clearest example of this is when a near-spherical cell is taken from suspension and placed on an isotropic and homogeneous flat substrate: its shape changes drastically in a process known as cell spreading due to a combination of energetically favorable surface adhesion and costly remodeling of its cytoskeleton (15, 16). There are distinct initial fast passive spreading phase (17, 18), and the subsequent slower active (energetically costly) spreading phase (19–21).

A symmetry-breaking pattern of membrane protrusions develops in the plane of attachment as the cell flattens during spreading. Most of these protrusions form towards the end of cell spreading: Johnston et al. (22) found that lamellipodia developed in fibroblasts after 30 minutes of spreading on fibronectin substrate. In comparison, key experiments by Fouchard et al. (23), and others (16, 24), suggest that integrin-mediated adhesion receptors begin to cluster around 3 minutes after initial contact with substrate. Here we must distinguish between 'mechanosensors' (or equivalently, the individual protein complexes with integrin at the distal end, binding to F-actin at the proximal end, providing the force chain from the substrate to the pulling actin filament, schematically drawn in Fig. 1), and the growing clusters of these individual mechanosensors (developing from nascent into full focal adhesions, where they are laterally bound into compact clusters).

Time-lapse immunofluorescence imaging (23, 24) shows that nascent focal adhesions (FAs) first develop once the cell has reached a particular shape of a spherical dome, and initially localize near the edge of the contact area. It also appears that clustering occurs with a specific length scale around the edge. The scenario is shown schematically in Fig. 2.

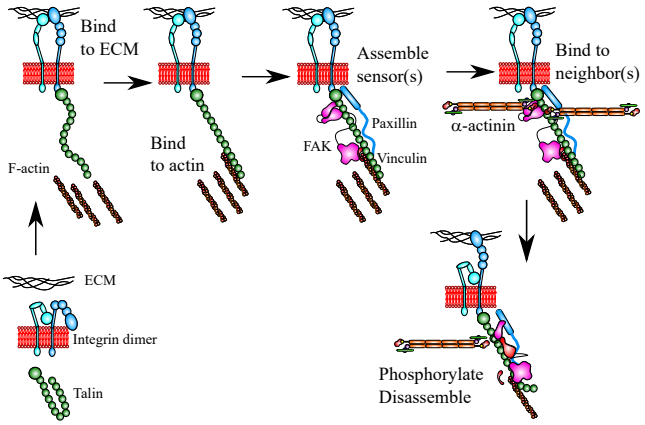

Figure 1: Sketch of a possible mechanism for the 5-step assembly of a mechanosensing complex, from Bell et al. (16). The following stages must occur and could limit the rate of sensor formation: integrin must be activated and bind to the ECM for adhesion to occur, talin must bind to F-actin (with paxillin and vinculin participating in the complex) for the force chain to form, the focal adhesion kinase (FAK) sensor is incorporated into the force chain (27), and neighboring sensors must interact to form a cluster. We suggest that α-actinin could be an appropriate mediator of nearest-neighbor interactions (28). Mechanosensors can only start to aggregate after a large proportion of them have formed, and the bridging protein could reach across to the neighbors.

Guo and Levine (25, 26) examined the development of spatial patterns of aggregates of cell-surface receptors, and showed that simple nearest-neighbor interactions between sensors arranged as a lattice gas lead to a phase transition when a uniform receptor distribution starts to aggregate into macroscopic clusters. Here we will find a similar phenomenon with clustering mechanosensors on the cell adhesion edge. The expansion of the cell-ECM contact area during spreading complicates the analysis of sensor aggregation. As the cell flattens, the lattice size continuously increases, which results in a decrease in the average sensor concentration, but also an increase in the number of possible arrangements of the sensor distribution. Hence, a phase transition can occur within a spreading cell, in our case driven by the competition between the decreasing sensor density and their attractive nearest-neighbor interaction that promotes closer proximity.

2.1 Cell shape changes during spreading.

When the cell comes in contact with a plane surface covered with ECM proteins, a small portion of the cell initially anchors to the substrate, possibly by

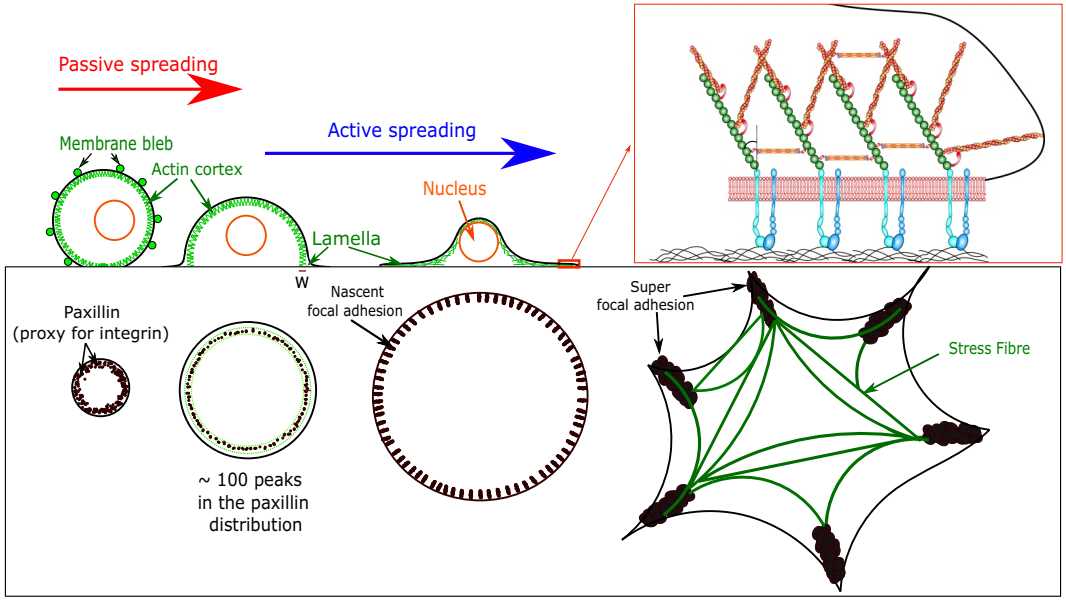

Figure 2: Upper panels: side-on sketch of a cell spreading on a 2D ECM surface. The cell settles by sedimentation, passive spreading and then active spreading (29). This results in a balance between adhesion energy and acto-myosin cortex deformation at first, followed by a protrusive force exerted by F-actin polymerization and transduced at focal adhesions (inset on the right). Lower panels: a view from above on the increasing cell-ECM contact area during spreading. As observed by Fouchard et al. (23), mechanosensors aggregate into FAs during cell spreading. After cell spreading, on sufficiently stiff substrates, FAs may aggregate further into super-FAs at fibronexi connected by large actin stress fibres (rightmost sketch).

hydrophobic or Van der Waals interactions (17, 30); this corresponds to Phase I of spreading as classified by Khalili and Ahmad (29). The cell membrane contains a large number of receptors which participate in binding to ECM ligands (31). These receptors then provide an added surface tension and serve as an energy source for the deformation of the cortex that takes place at the start of cell spreading. This process does not require the cell to expend any energy in the form of ATP-dependent protein polymerization or myosin motor action. This 'passive spreading' corresponds to Phase II of cell spreading following the classification (29). On sufficiently stiff substrates, this is subsequently followed by the 'active spreading' phase (21), or the Phase III (29); it lasts longer and involves slower spreading until the flattened cell reaches its maximal area. The rate of these processes depends on temperature due to the internal thermally-activated processes (16).

Simple physical models account well for these phases. Passive spreading matches the spreading of a composite viscous drop (18, 32). Active spreading involves a combination of viscous dissipation from the partial disassembly of the cortex, and the flow of cell material from F-actin polymerization (19).

Note that thermal fluctuations have a negligible effect on the shape of the cell during spreading. The combined effect of the acto-myosin cortex and bleb formation (15) is to create a membrane tension, which only permits small thermal fluctuations about a spherically symmetric shape of a eukaryotic cell in planktonic suspension. One can estimate the size of typical membrane fluctuations: $< 25nm$, if we assume that a tense giant unilamellar vesicle (GUV) is a good model for a cell in suspension. Once the cell adheres to a surface, the thermal membrane fluctuations are even smaller (reduced to the sub-nm scale) and can be ignored (33).

2.2 Interactions between mechanosensors.

The late stage of cell spreading on a flat substrate has many membrane protrusions. This angular shape is essential for biological function: for instance, on stiff substrates, fibroblasts may differentiate into myofibroblasts in order to participate in fibrosis and wound healing (34, 35). These cells display a small number of super-focal adhesions (36), which help set up long-lived acto-myosin stress fibres and maintain a large tension throughout (37), as illustrated in Fig. 2.

However, an initial angular shape pattern appears prior to these large-scale developments, during the

spreading process itself. The integrin-mediated adhesion complexes from Fig. 1 are amongst the best studied adhesive organelles (38, 39). Dynamic actin filaments pull against the complex, transmitting a local force across the cell membrane to the substrate. In the fully spread cell, macroscopic FAs are large aggregates of integrin complexes bound to a large number (over 50) of cytoplasmic proteins. Notably, fully-developed FAs contain vinculin, talin, paxillin, zyxin, α-actinin, VASP, FAK, phosphotyrosine proteins, integrin and others (40). We note that the concentration of constituting proteins (paxillin, talin, etc.) near the cell membrane is quite small at the start of cell spreading (41), but easier to detect in developed FAs.

Fouchard et al. (23) measured the paxillin distribution in spreading fibroblasts as a proxy for integrin mechanosensors. They showed that a spatial pattern with a specific aggregation length scale develops near the edge of the growing contact area after about 3 minutes of spreading. The cell was nearly hemispherical by this point. The component proteins of a mechanosensor are recruited to the membrane sites in this time according to (fast) diffusion, and a (much slower) binding kinetics. Bell et al. (16) found that a 5^{th} order kinetics determines the population-average average time when the spreading cell becomes hemispherical. This suggests that 5 thermally-activated steps are involved in the mechanosensor assembly, as sketched in Fig. 1.

Therefore, individual mechanosensors have to be assembled some time before the cell reaches the hemispheric configuration, and bound clusters start to form around this time; a mechanism for their aggregation would require a geometry-related transition between a uniform and heterogeneous distribution of individual mechanosensors. Fouchard et al. (23) suggest that the switch corresponds to the hemispheric configuration, but we do not see any reason for this observed criterion to be anything other than coincidental for the specific experimental situation. Sun et al. (39) suggested that this aggregation might occur via a kinetic mechanism, where the integrin-ECM binding would bend the glycocalyx around an adhesion site and thereby create a long range potential well within which mechanosensors would aggregate. This would to aggregation at a low spatial frequency, contrary to the large number (order 100) of nascent FAs found in experiments (23, 24).

Our proposed mechanism of mechanosensor interaction via bridging by mediating protein naturally accounts for the time lag between the formation of the individual mechanosensors and their clustering into nascent FAs. Should a short-range interaction be in play, one of constituents of the talin-bound cytoplasmic plaque would then mediate such an attractive interaction. α-actinin is a possible candidate for this: it is structurally symmetric and binds as a dimer to components of the protein plaque (28). The $36nm$ long α-actinin molecule (42) is of the right length to mediate a direct interaction between mechanosensors. Regardless of the nature of the molecular link (whether via α-actinin, or another multi-functional protein, e.g. vinculin), such a direct short-range attractive interaction is only active at distances comparable to the size of a mechanosensor. They can be modeled as simple nearest-neighbor interactions in a lattice gas model of the kind we develop below.

2.3 Localization of nascent focal adhesions.

But where does the cluster aggregation take place? Paxillin, a component of the talin-mediated force chain of the individual mechanosensor bound to integrin, is found at a high concentration very near the edge of the cell-ECM contact area after 3 minutes of spreading, that is, when the cell has reached a hemispherical shape (23, 24). This in turn suggests that integrins preferentially arrange themselves along the edge of this contact area. The true mechanism for the recruitment of integrin to the leading edge of the cell-ECM contact area is probably quite complex, but likely benefits from several cooperating processes, which help to determine both the spatial localization of the adhesions and their recruitment at the start of active spreading.

The energetic cost of bending the membrane is reduced by the presence of a receptor, promoting receptor localization in regions of high membrane curvature. The most curved region of the cell membrane is clearly at the edge of the cell-ECM contact area. Integrins progressively migrate via a succession of unbinding, fast diffusion and preferential binding to the edge of the cell-ECM contact area. Because of this, we would expect the integrin concentration to increase at the edge of this area on a ring, which we will henceforth dub the '*contact ring*'.

An estimate of the integrin-ECM binding force due to membrane curvature is useful to check whether this effect is relevant. When the leading cell edge extends by a distance dL_t, additional membrane material is added in a region of high curvature. This will require work $dW \approx f_0 dL_t$ and extends the membrane into a ring of size $dA = 2\pi R_{\text{cell}} dL_t$. The width of the leading edge is measured at $w_{\text{leading edge}} \approx 150nm$ (43), so the energetic cost of the additional membrane will be $dE = \frac{1}{2} B c^2 dA = \pi B R_{\text{cell}} / R_t^2 dL_t$, where B is the bending modulus, and c is the curvature of the membrane at the leading edge: $c \approx 1/w_{\text{leading edge}}$. This approximation becomes good when the cell has a spread radius of $1\mu m$ or more. The membrane bending modulus is known to be $390 k_B T$ in the presence of talin, and $70 k_B T$

without (44), so an estimate of $B \approx 100 k_B T$ seems reasonable. Equating $dW = dE$ gives a total force due to the membrane curvature at the edge of the contact area. To obtain the force per integrin, we scale to the width of each integrin mechanosensor complex ($w_{\text{complex}} \approx 40nm$), to give:

$$f_{0,\text{per complex}} \approx \frac{4\pi B w_{\text{complex}}}{w^2_{\text{leading edge}}} \approx 40pN \ . \qquad (1)$$

Kong et al. (45) have measured the integrin catch bonds to be most stable near this force value. Membrane curvature therefore stabilises integrin-matrix binding within a distance of the order of $w_{\text{leading edge}}$ of the edge of the cell. This argument supports a developing contact ring of the kind that we consider here.

The contractility of cytoskeleton applies the maximum tension, and increases the load on each sensor near the contact ring. This strengthens the integrin-matrix catch bonds and increases the residence time of the mechanosensor complexes within the thin intersectional area between the ECM plane and the out-of-plane cytoskeleton. We suggest that these mechanisms together help to explain why the paxillin/integrin distribution has a maximum on the contact ring at the start of active spreading. Note that the synthesis of new proteins is slow relative to the spreading process (in tens of minutes to an hour). Because of this, the number of mechanosensor complex constituents does not appreciably change throughout the initial phases of spreading. Consequently, we will henceforth assume that the number of mechanosensors found within this contact ring is a constant number N once the cell has spread beyond a critical radius.

2.4 A note on turnover

The question of mechanosensor aggregation is complicated by the turnover of integrin-talin-FAK mechanosensors (46–48). When the sensor opens under force (27), it changes the conformation of FAK to allow phosphorylation and initiate the signaling pathways. This irreversibly changes the nature integrin-talin or the talin-FAK bonds (49), and detaches the protein complex from the integrin anchor. However, it is unreasonable to expect the entire complex to fully disassemble after this. More likely, it stays mostly intact and can bind anew to free inactive integrins, after FAK autoinhibition.

Regardless of the exact dynamics of the cytoplasmic plaque being bound to integrin, the problem is much more tractable if we assume that key parts of the mechanosensing complex remain intact even when FAK, talin and integrin are in the process of reverting back to their native conformations. Indeed, for short-range interactions, the molecule which mediates the nearest-neighbor interaction could well be bound to some of the proteins found in the region of talin which is available to bind in both its closed and open configurations. In that case, we would expect the binding between neighboring mechanosensors to be roughly independent of whether or not the sensor is primed, or open (this certainly is the case in the developed FAs). In contrast, the kinetics of aggregation due to a long-range interaction (39) would be seriously affected by integrin decoupling, as the membrane deformation due to the presence of the mechanosensor would only come into effect when the sensor is fully assembled.

3 The model and methods

Two mechanosensing complexes can interact directly at short range. α-actinin is a prime candidate to mediate this interaction because it is a symmetrical molecule which can bind as a dimer, it interacts with the load-bearing FA proteins vinculin and talin, and it is found close to where mechanosensors form due to its role as a cross-linker within the actin cortex.

3.1 Thermodynamic mechanism for aggregation

The formation of nascent FAs (lasting minutes) during cell spreading is a much faster process than and protein synthesis (up to an hour), but is much slower than diffusion across 1-10μm distances. This motivates modeling the mechanosensors within a cell as a thermally equilibrated distribution of a fixed number N of individual sensors located along the contact ring. The typical lifetime of about 20s for integrin-ECM bonds complicates this picture a little, but should not noticeably affect aggregation kinetics over times of the order of a few minutes.

We model the contact ring as a 1D lattice with cyclic boundary conditions. To replicate gradual cell spreading, we adiabatically increase the length of the ring (or, equivalently, the number of equally-spaced lattice sites L). Fig. 3 schematically illustrates the situation.

This sort of modeling is typical in a numerical approach (50, 51). The simplest possible model of the interaction is an adaptation of the Ising model, as considered by Guo and Levine (25):

$$H = -J\Sigma_{\langle ij \rangle} n_i n_j \qquad (2)$$

where $\Sigma_{\langle .. \rangle}$ indicates a sum over nearest-neighbor pairs. The variable n indicates the state of the sensor, which in our case is the occupation number:

$$n_i = \begin{cases} 1 & \text{sensor present} \\ 0 & \text{sensor absent} \end{cases} \ . \qquad (3)$$

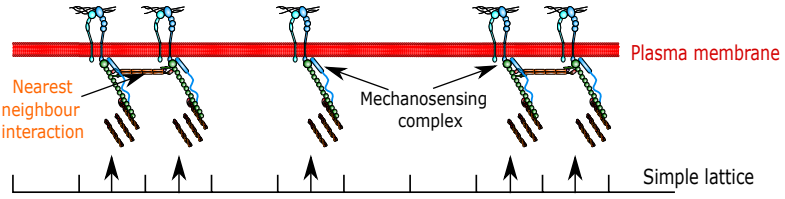

Figure 3: Schematic representation of the 1D lattice model of nearest-neighbor sensor interactions. The sensors aggregate along the contact ring between the spreading cell and the adhesive surface to which it is attached.

The constant J indicates the binding energy of nearest-neighbor interaction in this lattice model, whose exact value likely depends on cell type.

With these simplifications in hand, we will calculate the Ginzburg-Landau action (the free energy of the mechanosensor density distribution) and examine the spatio-temporal evolution of the distribution of mechanosensors located on the contact ring.

3.2 Sensor interaction model

We assume the length of the contact ring between a cell and an adhesive surface to be constant for any process which occurs on a much shorter timescale than cell spreading (seconds rather than minutes). Here, this implies that the number of lattice sites L is constant on the time scale of thermal equilibration. Using this simplification, we can closely mirror the derivation for the classical Ising model over a sufficiently short time interval.

The single-molecule partition function for the lattice gas model with Hamiltonian H from Eqn. (2) is:

$$Z_i = \Sigma_{n_i=\{0,1\}} e^{-\beta(-\frac{1}{2}J\Sigma_{\langle j\rangle} n_j)\cdot n_i} \ , \qquad (4)$$

where the sum runs over all of the L sites around the ring, and $\beta = 1/k_B T$, as usual.

The full partition function is the product of L partition functions for each site, subject to the constraint $N = \Sigma_i n_i$ of the constant total number of individual sensors. The Supplementary Information (part A) gives the calculation of this partition function using the auxilliary fields method. We need a variable on each site: ϕ_i, whose expectation value can be identified with the average occupation of a site, which is the order parameter: $\langle \phi_i \rangle = \langle n_i \rangle$. This identifies the discrete field ϕ_i as the mechanosensor concentration at site i. We will later transform this into a continuous density $\phi(s)$ which depends on a the position s around the contact ring. The calculation of $Z_{\rm tot} = \delta(\Sigma_i n_i - N)\Pi_{i=1}^{L} Z_i$ is exact, but rather unwieldy. We will have to make several strong approximations in the next section to proceed towards a manageable form for the effective action $S[\phi]$.

Key approximation 1: high occupancy.

Near the start of spreading, we assume that the majority of sites on the contact ring of an initially small footprint are occupied by a mechanosensor, so N can be assumed to be the same order as L. We feel this is a reasonable assumption, as at the very early stages of cell spreading the contact ring is very small and the cell has many more integrin units available than there is room on the ring; this will change as the cell spreads more and more. This assumption means that the probability of a single site being in the 'filled' state (i.e. contain a mechanosensor complex) is much greater than that of being in the 'empty' state. This gives the following condition (see Supplementary, part A):

$$e^{(\beta h + m + x_a)} = \frac{1}{L-N} \ \Sigma_{i=1}^{L} e^{-x_i'} \gg 1. \qquad (5)$$

As expected, this is a large quantity if the number of sites and the number of sensors are both large.

Key approximation 2: small non-uniformity.

Initially, the contact ring is fully populated with a density uniform $\phi = 1$, but as the ring grows the average density falls. Here we look for the initial instability when a small inhomogeneous fluctuation of this density starts growing, eventually leading to a densely packed FA. Using this approximation, we perform the series expansion of the action in terms of the fluctuation of the density, $\phi' = \phi - N/L$ (where the average density of sensors is $\langle \phi \rangle = N/L$), details in Supplementary, part B.

In Supplementary part C, we obtain the effective action $S[\phi]$, transform it into continuous Fourier space, make it continuous, and finally transform it back into real space (the last operation generating the spatial gradients). This effective free energy has recognizable features of the Ginzburg-Landau theory, where we retain cubic and quartic terms in the order parameter

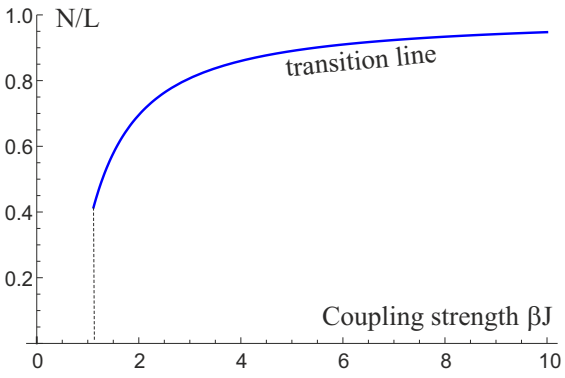

Figure 4: The 'phase diagram' of values of average sensor density N/L vs. the sensor interaction strength βJ, showing the transition line at which the coefficient r_0 from Eqn. (7) changes sign, and the clustering instability becomes possible. r_0 remains positive for βJ smaller than the critical value close to 1, as labelled on the plot.

expansion:

$$S_{\Lambda_0}[\phi'] = \int_0^L ds\Big[\frac{r_0}{2}\phi'^2(s) + \frac{c_0}{2}[\nabla\phi'(s)]^2 + \frac{t_1}{3!}\phi'^3(s) + \frac{u_1}{4!}\phi'^4(s) + \frac{u_2}{4!}\phi'^2(s)\Big(\int ds'\phi'^2(s')\Big)\Big] \ , \quad (6)$$

where L is the length of contact ring perimeter, all lengths are scaled by the size of the individual sensor a, and the coefficients are defined in Supplementary, part C. Specifically, the two quadratic-order coefficients take the form, Eqn. (C.9):

$$r_0 = 2\beta J(1 - 2g_2\beta J) \ ; \quad c_0 = 4g_2\beta^2 J^2 - \beta J \ , \quad (7)$$

with

$$g_2 = \frac{(3 - 2N/L)}{(N/L - 2)^2} - \frac{N}{L} \ .$$

We see that the control parameter (replacing the temperature in the classical theory of phase transitions) is the ratio N/L, which starts at 1 when the small cell adhesion ring first forms, and then diminishes as the cell spreads and the ring perimeter L grows. The gradient coefficient c_0 remains positive, but the main 'control' coefficient r_0 could become negative (thus causing the instability of the homogeneous density distribution around the adhesion ring) at a critical value of N/L, which depends on the coupling strength βJ. Note that near this critical point c_0 takes an approximately constant value $c_0 = 2g_2\beta^2 J^2$. At large βJ (i.e. when the sensors are strongly bound across) the instability occurs almost immediately below $N/L = 1$, while for $\beta J < 1$ the coefficient r_0 remains positive for all N/L and no instability occurs, see Fig. 4.

4 Results and comparison with experimental data

4.1 Spatial frequency of fluctuations

In the immediate vicinity of the critical point, the quadratic-order terms in the density of sensor concentration fluctuations ϕ' are much larger than all of the higher order terms. The action (effective free energy) written in Eqn. (6) can therefore be substantially simplified in the vicinity of the critical point:

$$S_{\Lambda_0}[\phi'] = \int_0^L ds\Big[\frac{r_0}{2}\phi'^2(s) + \frac{c_0}{2}[\nabla\phi'(s)]^2\Big] \ . \quad (8)$$

The time-dependence of the concentration fluctuation can be described by the Cahn-Hilliard equation (52), which takes the following form near the critical point:

$$\frac{\partial\phi'}{\partial t} = D\nabla^2\Big(r_0\phi' - c_0\nabla^2\phi'\Big) \ , \quad (9)$$

where in our case D is the diffusion coefficient of the sensor along the ring (keeping in mind the factor of a^2 that needs to be added if we were to use the proper dimensional units). The behaviour of the concentration fluctuation is subject to the boundary conditions:

$$\nabla\phi'(0,t) = \nabla\phi'(L,t) = \nabla^3\phi'(0,t) = \nabla^3\phi'(L,t) = 0 \ . \quad (10)$$

A well-known solution satisfies these boundary conditions:

$$\phi'(s,t) = \tfrac{1}{2}A_0(t) + \Sigma_k A_k(0) e^{-D\frac{k^2}{4}\left(r_0 + \frac{c_0 k^2}{4}\right)t}\cos\left(\tfrac{ks}{2}\right) \ , \quad (11)$$

where k is the wavevector, directly related to the number m of peaks in the azimuthal modulation of sensor concentration: $k = 2\pi m/L$.

The fastest growing wavenumber, which corresponds to the oscillation length scale that maximizes the exponential term above, is:

$$k_{\max} = \sqrt{-2r_0/c_0} \ . \quad (12)$$

The critical mode number, for the largest spatial frequency at which the exponential term could grow with time is

$$k_{\rm crit} = 2\sqrt{-r_0/c_0} \quad (13)$$

(see Eqn. (7) for the values of r_0 and c_0, and Fig. 4 showing when r_0 becomes negative).

Which of these two wavevectors determines the timescale and spatial patterns of nascent FA formation? These equations are only accurate near the critical point; as the cell spreads, the control parameter $-r_0(L,N)$ increases, so both the fastest growing mode and the critical mode increase. Once the limit of small fluctuations no longer applies, we will need to find the timescale for mode growth in a different manner. In particular, low frequencies (large spatial periodicity) take

a long time to grow and develop. We expect that the limit of small fluctuations will apply for all low modes until one of the higher frequency modes, namely the fastest growing mode at a particular spreading time, can no longer be well described by the small fluctuations approximation. In terms of the Ginzburg-Landau action in Eqn. (6), aggregates with well-defined boundaries form and their sharp edges result in a smaller energetic cost from the gradient term $\frac{1}{2}c_0[\nabla\phi'(s)]^2$. This means that we expect the growth rate of the fastest growing mode to increase once aggregates start to form. In Supplementary part D we verify that the effective action (free energy) remains stable when fluctuations grow larger, which makes the coarsening analysis valid. In turn, this will result in Cahn-Hilliard coarsening at the specific frequency of the mode which grows fastest when fluctuations are no longer small. Let us find this mode.

4.2 Time until a mode becomes unstable

First, we must determine how long it takes a mode to become unstable after the cell passes the critical point. This depends crucially on a combination of the spreading speed and the radius of the cell at the phase transition. In Supplementary part E, we carry out a series approximation of the fastest growing mode number near the critical point. This shows that modes initially grow proportionally to the square root of changes in the size of the lattice. In other words, the mode number m is directly proportional to the square root of changes in the radius of the cell, and also to the square root of the time elapsed since the cell was at our phase transition.

Now we must return to proper dimensional length scales, and thus keep track of the powers of a. The result of this series expansion (performed in Supplementary part E) is that we have the following approximation:

$$m(t_{\text{destabilise}})^2 \approx \Psi(\beta J)\left(\frac{t_{\text{destabilise}}2\pi\dot{r}_{\text{spread}}}{a}L_{\text{critical}}\right) , \tag{14}$$

where $\dot{r}_{\text{spread}}$ is the rate of spreading of the radius of the cell, and $\Psi(\beta J)$ is a complicated function obtained from the series expansion of the mode number about the critical point for small changes $\Delta L(t)$ of the lattice size. We show in Supplementary part E that the series approximation is good for an increase in spread cell area of $5-10\%$. This will therefore apply to the initial aggregation of mechanosensors.

4.3 Mode growth time

For the fastest growing mode, $r_0 = -c_0k_{\text{max}}^2/2$, so we can find the time that it takes to grow by substituting into the exponent in the solution of the Cahn-Hilliard equation: Eqn. (11):

$$e^{-D\frac{k^2}{4}\left(r_0+\frac{c_0k^2}{4}\right)t}\Big|_{\text{max}} = e^{D\frac{k^4c_0}{16}t} \tag{15}$$

Substituting the constants r_0 and c_0, and recovering the proper dimensional length scales via a, we find that the growth time of the mode becomes:

$$t_{\text{grow}} = \alpha\frac{L^4a^2}{2\pi^4m^4Dg_2(\beta J)^2} , \tag{16}$$

where α is a proportionality constant of order 1.

Goennenwein et al. (53) used FRAP experiments to find that free integrin diffusion coefficients were of the order of $D_{\text{integrin}} = 0.6\mu m^2/s$. Assuming that the diffusion time of a mechanosensing complex is comparable to the integrin diffusion time, we may numerically evaluate the above expression with $\lambda_{\text{max}} = 2\pi r_{\text{spread}}/m_{\text{max}}$ for a typical radius of the spread cell r_{spread} at the time of the formation of the nascent adhesions. We must bear in mind that in doing this we have probably somewhat overestimated the mechanosensor diffusion coefficient.

4.4 Number of nascent adhesions

The fastest growing mode is determined by a combination of these two times: the time that it takes the cell to spread to a radius $L_0 + \Delta L$ at which the m^{th} mode becomes unstable, where L_0 is the smallest radius at which the critical mode is unstable, and the time that it takes the m^{th} mode to grow. We saw in Eqn. (14) that the spreading time until mode m becomes the fastest growing mode is proportional to m^2 for small changes in cell size. As for the second time, we saw in Eqn. (16) that the growth time of the mode is proportional to m^{-4}. Thus, the total time for a mode to grow is:

$$t_{\text{tot}} = t_{\text{destabilise}} + t_{\text{mode growth}} = K_1m^2 + K_2m^{-4} \tag{17}$$

where K_1 and K_2 are the proportionality constants in Eqs. (14), (16). The total time is minimized when:

$$\frac{dt_{\text{tot}}}{dm} = 2K_1m - 4K_2m^{-5} = 0 \tag{18}$$

$$\Rightarrow m^* = \left(\frac{2K_2}{K_1}\right)^{1/6} \tag{19}$$

The mode corresponding to the number of nascent adhesions is the solution to this equation. We make the proportionality constants explicit and find that the number of nascent adhesions is

$$m^* = \left(\alpha\frac{2L_{\text{critical}}^5a}{\pi^3Dg_2(N,L)(\beta J)^2}\Psi(\beta J)\dot{r}_{\text{spread}}\right)^{1/6} \tag{20}$$

This is the main prediction of this paper.

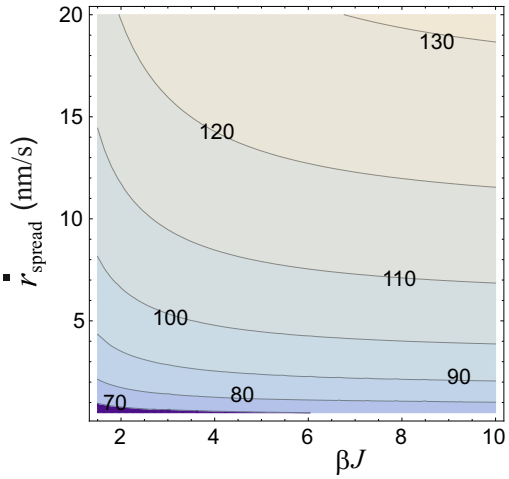

Figure 5: Contour plot of the predicted number of nascent focal adhesions m^* as a function of interaction energy (scaled by the energy of thermal fluctuations) and the spreading rate of the radius of the cell during the active spreading phase (in nm/s). We therefore predict that a large number of cells should display a hundred or so nascent focal adhesions after these sensors begin to aggregate. Note that the predicted number of nascent focal adhesions is very similar for a large range of spreading velocities.

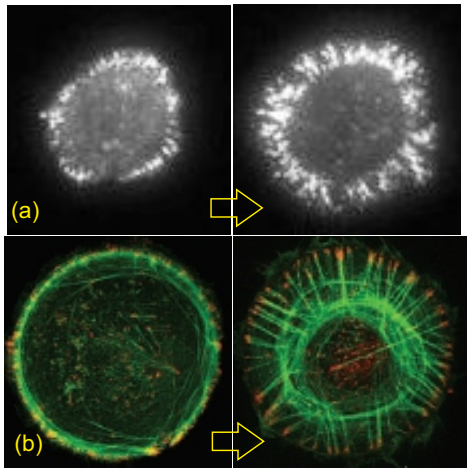

Figure 6: Images showing the transformation of the density of adhesion complexes (labelled by fluorescence of paxillin) as the contact ring expands on cell spreading. Images (a) are from Fouchard et al. (23), and images (b) are from Tee et al. (24), with permission.

To make comparisons with experiments we use the following parameters: mechanosensor spacing $a = 40nm$, spread radius $r_{\text{spread}} = 18\mu m$ (23), lattice length at the phase transition $L_{\text{critical}} = 2\pi r_{\text{spread}}/a \approx 2800$, the diffusion constant $D = 0.6\mu m^2/s$, and proportionality constant $\alpha = 1$ for simplicity's sake. Fouchard et al. (23) measure the spreading rate after the transition to active spreading and it is decently approximated by a constant $\dot{r}_{\text{spread}} \approx 0.005\mu m/s$ (which depends on temperature, substrate mechanical properties, etc.). While $\dot{r}_{\text{spread}}$ may be constant for a given cell and spreading phase, it will vary across cultures and cell types, so it does not make sense to fix its value.

Thus, we vary the spreading rate (around the known experimental values) as well as the interaction energy J, and plot the resulting mode number m^* – which also corresponds to the number of nascent focal adhesions – in Fig. 5. The number of nascent FAs is typically of the order of 100 for a wide range of interaction energies and spreading rates. Obviously, there is a large uncertainty in this value, but it is worth noting that due to the sixth-root dependence of the mode number on its constituent proportionality constants in Eqn. (20), any one of our parameter values would typically have to be wrong by a factor of 10^6 to lead to a 10 times fewer or more focal adhesions. Such a discrepancy seems unlikely.

Figure 6 illustrates experimental observations of spreading cells in the early regime we are studying in this work. It is clear that in both cases the number of nascent mechanosensor clusters (determined by proxy from the concentration of paxillin) is of the order of 100 (possibly slightly fewer). Their number might already have decreased due to Cahn-Hilliard coarsening between developed nascent adhesions by the time of the right-hand picture, but is in line with our theoretical predictions.

5 Discussion and conclusions

Recent biological data lends credence to the idea that clustering of integrin-mediated mechanosensors found in focal adhesions is responsible for the development of initial azimuthal inhomogeneity. In particular, we suggest the possibility that a thermodynamic mechanism relying on short-range protein bridging plays a substantial role in cell spreading. We identify the ring at the intersection of the cell basal plane and the out-of-plane acto-myosin cortex as a possible location for the recruitment and the aggregation of the constituent proteins of the mechanosensor complex.

The main appeal of this approach, namely that it involves an analytically tractable 1D lattice model, is also its principal limitation. To approach reality somewhat further, an alternative would be to computationally examine the related 2D lattice problem, as in e.g. (51). Arguably, this would require even more assumptions, including concerning the width of the cortex,

the width and fluctuations of the leading edge, integrin binding and diffusion kinetics and so on. And even if successful, such an approach would most likely not qualitatively change the predictions of the simple aggregation kinetics, but merely yield a phase transition at a somewhat different sensor concentration and possibly result in a slightly different spatial frequency of aggregation.

This thermodynamic mechanism may potentially cooperate with a kinetic mechanism of receptor clustering (39), which relies on long-range mechanosensor-induced membrane deformations to attract other bound integrins. Although both mechanisms involve very different interactions, it is not immediately clear how to distinguish their predictions – not only because of the lack of accurate biological data, but because many of these are similar: both predict that mechanosensors will aggregate on a particular length scale for instance.

One could potentially differentiate between the two models by more accurately measuring the onset time of the formation of nascent adhesions. The thermodynamic model would be favoured if this aggregation time does not coincide with a particular cell shape (*e.g.* a quasi-hemispherical cell). One might also be able to test the validity of the kinetic mechanism by measuring the membrane deformation stresses around bound integrins in order to determine the strength and width of the kinetic well.

The aggregation of integrin-mediated mechanosensors into dense clusters has clear consequences for the subsequent evolution of the cell shape during the remainder of spreading. The formation of FAs offers anchors for the extension of the lamella via actin polymerization. Newly formed actin filaments push against ECM-bound nascent FAs and exert a protrusive force on the membrane, which leads to further spreading and sets up a retrograde flow of actin behind the adhesions. This in turn helps set up a clear radial directionality to the growth of FAs, which become long and radially-oriented. Therefore, while a 1D model around the adhesion contact ring was useful in examining the initial aggregation at the start of the active spreading, it is insufficient to understand their growth and decay towards the later stages of cell spreading. Nonetheless, studies clearly show that the angular distribution of the initial pattern, which we investigated in this work, correlates strongly with the subsequent distribution of FAs (23).

Our approach does not require detailed knowledge about biochemical reactions or mechanical traction forces. Both of these are implicit in the interaction energy between neighboring sensors. It is only because the cell is so highly symmetrical (round) during the initial stages of spreading, and because the azimuthal aggregation of sensors does not involve gradients of either chemical or mechanical properties of interest, that we are able to keep knowledge of these cellular parameters implicit. Radial processes during cell spreading cannot be analyzed in such a manner: the changing shape of the cell, or the radially-oriented maturation of FAs after the nascent stage, require a detailed understanding of the manner in which chemical and mechanical quantities change across the cell-matrix contact area.

Finally, we suggest that a similar contact ring might arise on either side of a cell-cell junction between two interacting eukaryotic cells. A similar mechanism might lead to cadherin-based sensors aggregation into adherens junctions after cadherin-actin bonds have developed (54, 55). This might have an even more biologically relevant role, as the adhesion surface between two cells is much more naturally two-dimensional than an in-vivo ECM surface.

Author contribution

Both authors conceived the idea, carried out different elements of data analysis and wrote the paper.

Acknowledgements

The authors acknowledge many helpful discussions with Sam Bell, Theresa Jakuzeit, Heidi Welch, and Camillo Moschner - who also proofread the manuscript. We are grateful to J. Fouchard, A. Asnacios, and A. Bershadsky for giving access to their experimental results, and critical discussions. This work has been funded by BBRSC DTP Cambridge (grant no. EP/M508007/1).

References

1. Chen, C. S., 2008. Mechanotransduction - a field pulling together? J. Cell Sci. 121:3285–3292.
2. Discher, D. E., 2005. Tissue cells feel and respond to the stiffness of their substrate. Science (80-.). 310:1139–1143.
3. Engler, A. J., S. Sen, H. L. Sweeney, and D. E. Discher, 2006. Matrix Elasticity Directs Stem Cell Lineage Specification. Cell 126:677–689.
4. Janmey, P. A., J. P. Winer, M. E. Murray, and Q. Wen, 2009. The hard life of soft cells. Cell Motil. Cytoskeleton 66:597–605.
5. Vogel, V., and M. Sheetz, 2006. Local force and geometry sensing regulate cell functions. Nat. Rev. Mol. Cell Biol. 7:265–275.
6. Nelson, C. M., R. P. Jean, J. L. Tan, W. F. Liu, N. J. Sniadecki, A. A. Spector, and C. S. Chen, 2005. Emergent patterns of growth controlled by multicellular form and mechanics. Proc. Natl. Acad. Sci. 102:11594–11599.
7. Cove, D. J., 2000. The generation and modification of cell polarity. J. Exp. Bot. 51:831–838.
8. Bagorda, A., and C. A. Parent, 2008. Eukaryotic chemotaxis at a glance. J. Cell Sci. 121:2621–2624.

9. Lo, C.-M., H.-B. Wang, M. Dembo, and Y.-l. Wang, 2000. Cell movement is guided by the rigidity of the substrate. Biophys. J. 79:144–152.
10. Isenberg, B. C., P. A. DiMilla, M. Walker, S. Kim, and J. Y. Wong, 2009. Vascular Smooth Muscle Cell Durotaxis Depends on Substrate Stiffness Gradient Strength. Biophys. J. 97:1313–1322.
11. Swaney, K. F., C.-H. Huang, and P. N. Devreotes, 2010. Eukaryotic Chemotaxis: A Network of Signaling Pathways Controls Motility, Directional Sensing, and Polarity. Annu. Rev. Biophys. 39:265–289.
12. Parsons, J. T., A. R. Horwitz, and M. A. Schwartz, 2010. Cell adhesion: integrating cytoskeletal dynamics and cellular tension. Nat. Rev. Mol. Cell Biol. 11:633–643.
13. Zaidel-Bar, R., and B. Geiger, 2010. The switchable integrin adhesome. J. Cell Sci. 123:1385–1388.
14. Hartman, C. D., B. C. Isenberg, S. G. Chua, and J. Y. Wong, 2016. Vascular smooth muscle cell durotaxis depends on extracellular matrix composition. Proc. Natl. Acad. Sci. 113:11190–11195.
15. Bou Daher, F., Y. Chen, B. Bozorg, J. Clough, H. Jönsson, and S. A. Braybrook, 2018. Anisotropic growth is achieved through the additive mechanical effect of material anisotropy and elastic asymmetry. Elife 7.
16. Bell, S., A.-L. Redmann, and E. M. Terentjev, 2019. Universal Kinetics of the Onset of Cell Spreading on Substrates of Different Stiffness. Biophys. J. 116:551–559.
17. Bruinsma, R., and E. Sackmann, 2001. Bioadhesion and the dewetting transition. Comptes Rendus l'Académie des Sci. - Ser. IV - Physics-Astrophysics 2:803–815.
18. Cuvelier, D., M. Théry, Y.-S. Chu, S. Dufour, J.-P. Thiéry, M. Bornens, P. Nassoy, and L. Mahadevan, 2007. The Universal Dynamics of Cell Spreading. Curr. Biol. 17:694–699.
19. Fardin, M. A., O. M. Rossier, P. Rangamani, P. D. Avigan, N. C. Gauthier, W. Vonnegut, A. Mathur, J. Hone, R. Iyengar, and M. P. Sheetz, 2010. Cell spreading as a hydrodynamic process. Soft Matter 6:4788.
20. Döbereiner, H.-G., B. Dubin-Thaler, G. Giannone, H. S. Xenias, and M. P. Sheetz, 2004. Dynamic Phase Transitions in Cell Spreading. Phys. Rev. Lett. 93:108105.
21. Dubin-Thaler, B. J., G. Giannone, H.-G. Döbereiner, and M. P. Sheetz, 2004. Nanometer analysis of cell spreading on matrix-coated surfaces reveals two distinct cell states and STEPs. Biophys. J. 86:1794–1806.
22. Johnston, S. A., J. P. Bramble, C. L. Yeung, P. M. Mendes, and L. M. Machesky, 2008. Arp2/3 complex activity in filopodia of spreading cells. BMC Cell Biol. 9:65.
23. Fouchard, J., C. Bimbard, N. Bufi, P. Durand-Smet, A. Proag, A. Richert, O. Cardoso, and A. Asnacios, 2014. Three-dimensional cell body shape dictates the onset of traction force generation and growth of focal adhesions. Proc. Natl. Acad. Sci. 111:13075–13080.
24. Tee, Y. H., T. Shemesh, V. Thiagarajan, R. F. Hariadi, K. L. Anderson, C. Page, N. Volkmann, D. Hanein, S. Sivaramakrishnan, M. M. Kozlov, and A. D. Bershadsky, 2015. Cellular chirality arising from the self-organization of the actin cytoskeleton. Nat. Cell Biol. 17:445–457.
25. Guo, C., and H. Levine, 1999. A Thermodynamic Model for Receptor Clustering. Biophys. J. 77:2358–2365.
26. Guo, C., and H. Levine, 2000. A statistical mechanics model for receptor clustering. J. Biol. Phys. 26:219–34.
27. Bell, S., and E. M. Terentjev, 2017. Focal Adhesion Kinase: The Reversible Molecular Mechanosensor. Biophys. J. 112:2439–2450.
28. Hamill, K. J., S. Hiroyasu, Z. T. Colburn, R. V. Ventrella, S. B. Hopkinson, O. Skalli, and J. C. Jones, 2015. Alpha actinin-1 regulates cell-matrix adhesion organization in keratinocytes: consequences for skin cell motility. J. Invest. Dermatol. 135:1043–1052.
29. Khalili, A., and M. Ahmad, 2015. A Review of Cell Adhesion Studies for Biomedical and Biological Applications. Int. J. Mol. Sci. 16:18149–18184.
30. Sackmann, E., and R. F. Bruinsma, 2002. Cell Adhesion as Wetting Transition? ChemPhysChem 3:262.
31. Lee, J. E., J. F. Kellie, J. C. Tran, J. D. Tipton, A. D. Catherman, H. M. Thomas, D. R. Ahlf, K. R. Durbin, A. Vellaichamy, I. Ntai, A. G. Marshall, and N. L. Kelleher, 2009. A robust two-dimensional separation for top-down tandem mass spectrometry of the low-mass proteome. J. Am. Soc. Mass Spectrom. 20:2183–2191.
32. Étienne, J., and A. Duperray, 2011. Initial dynamics of cell spreading are governed by dissipation in the actin cortex. Biophys. J. 101:611–621.
33. Monzel, C., and K. Sengupta, 2016. Measuring shape fluctuations in biological membranes. J. Phys. D. Appl. Phys. 49:243002.
34. Huang, X., N. Yang, V. F. Fiore, T. H. Barker, Y. Sun, S. W. Morris, Q. Ding, V. J. Thannickal, and Y. Zhou, 2012. Matrix Stiffness–Induced Myofibroblast Differentiation Is Mediated by Intrinsic Mechanotransduction. Am. J. Respir. Cell Mol. Biol. 47:340–348.
35. Hinz, B., 2009. Tissue stiffness, latent TGF-β1 Activation, and mechanical signal transduction: Implications for the pathogenesis and treatment of fibrosis. Curr. Rheumatol. Rep. 11:120–126.
36. Goffin, J. M., P. Pittet, G. Csucs, J. W. Lussi, J.-J. Meister, and B. Hinz, 2006. Focal adhesion size controls tension-dependent recruitment of α-smooth muscle actin to stress fibers. J. Cell Biol. 172:259–268.
37. Burridge, K., and C. Guilluy, 2016. Focal adhesions, stress fibers and mechanical tension. Exp. Cell Res. 343:14–20.
38. Burridge, K., and M. Chrzanowska-Wodnicka, 1996. Focal adhesions, contractility, and signaling. Annu. Rev. Cell Dev. Biol. 12:463–519.
39. Sun, Z., S. S. Guo, and R. Fässler, 2016. Integrin-mediated mechanotransduction. J. Cell Biol. 215:445–456.
40. Zaidel-Bar, R., M. Cohen, L. Addadi, and B. Geiger, 2004. Hierarchical assembly of cell–matrix adhesion complexes. Biochem. Soc. Trans. 32:416–420.
41. Mueller, S. C., T. Kelly, M. Z. Dai, H. N. Dai, and W. T.

Chen, 1989. Dynamic cytoskeleton-integrin associations induced by cell binding to immobilized fibronectin. J. Cell Biol. 109:3455–3464.
42. Sjöblom, B., A. Salmazo, and K. Djinović-Carugo, 2008. α-Actinin structure and regulation. Cell. Mol. Life Sci. 65:2688–2701.
43. Gabella, C., E. Bertseva, C. Bottier, N. Piacentini, A. Bornert, S. Jeney, L. Forró, I. F. Sbalzarini, J. J. Meister, and A. B. Verkhovsky, 2014. Contact angle at the leading edge controls cell protrusion rate. Curr. Biol. .
44. Simson, R., E. Wallraft, J. Faix, J. Niewohner, G. Gerisch, and E. Sackmann, 1998. Membrane bending modulus and adhesion energy of wild-type and mutant cells of Dictyostelium lacking talin or cortexillins. Biophys. J. .
45. Kong, F., A. J. García, A. P. Mould, M. J. Humphries, and C. Zhu, 2009. Demonstration of catch bonds between an integrin and its ligand. J. Cell Biol. 185:1275–1284.
46. Ballestrem, C., B. Hinz, B. A. Imhof, and B. Wehrle-Haller, 2001. Marching at the front and dragging behind. J. Cell Biol. 155:1319–1332.
47. Das, M., S. Subbayya Ithychanda, J. Qin, and E. F. Plow, 2014. Mechanisms of talin-dependent integrin signaling and crosstalk. Biochim. Biophys. Acta - Biomembr. 1838:579–588.
48. Goult, B. T., T. Zacharchenko, N. Bate, R. Tsang, F. Hey, A. R. Gingras, P. R. Elliott, G. C. K. Roberts, C. Ballestrem, D. R. Critchley, and I. L. Barsukov, 2013. RIAM and vinculin binding to talin are mutually exclusive and regulate adhesion assembly and turnover. J. Biol. Chem. 288:8238–8249.
49. Chang, F., C. A. Lemmon, D. Park, and L. H. Romer, 2007. FAK potentiates Rac1 activation and localization to matrix adhesion sites: A role for βPIX. Mol. Biol. Cell 18:253–264.
50. Lepzelter, D., O. Bates, and M. Zaman, 2012. Integrin Clustering in Two and Three Dimensions. Langmuir 28:5379–5386.
51. Foo, D. C. W., and E. M. Terentjev, 2018. Cooperative mechanosensitivity and allostery of focal adhesion clusters. Phys. Biol. 15:aa953d.
52. Cahn, J. W., 1961. On spinodal decomposition. Acta Metall. 9:795–801.
53. Goennenwein, S., M. Tanaka, B. Hu, L. Moroder, and E. Sackmann, 2003. Functional incorporation of integrins into solid supported membranes on ultrathin films of cellulose: Impact on adhesion. Biophys. J. .
54. Tsukita, S., S. Tsukita, A. Nagafuchi, and S. Yonemura, 1992. Molecular linkage between cadherins and actin filaments in cell—cell adherens junctions. Curr. Opin. Cell Biol. 4:834–839.
55. Yonemura, S., 2011. Cadherin-actin interactions at adherens junctions. Curr. Opin. Cell Biol. 23:515–522.